Associated conference: 5th International Small Sample Test Techniques Conference

Conference location: Swansea University, Bay Campus

Conference date: 10th - 12 July 2018

How to cite: Abendroth, M., & Zielke, H. 2018. Numerical investigation of the influence of friction in SPT experiments. *Ubiquity Proceedings*, 1(S1): 1 DOI: https://doi.org/10.5334/uproc.1

Published on: 10 September 2018

Numerical investigation of the influence of friction in SPT experiments

M. Abendroth [1,*], H. Zielke [2]

[1] TU Bergakademie Freiberg; martin.abendroth@imfd.tu-freiberg.de
[2] TU Bergakademie Freiberg; henry.zielke@imfd.tu-freiberg.de
***** Correspondence: martin.abendroth@imfd.tu-freiberg.de; Tel.: +49-3731-39-4132

Abstract: Virtually all SPT test stands, which are operated in different laboratories, cause contact between different parts of the SPT due to the technical design. These frictional influences can lead to erroneous test results since the force transmitted from the punch to the sample is reduced. This influence can be considerable, particularly in the case of creep tests at high temperatures. The present work analyses various typical experimental setups and the influence of inaccuracies in the setup on the test results. Finally, some requirements and suggestions for an optimized experimental setup are derived.

Keywords: small punch test; friction; finite elements

1. Introduction

The small punch test (SPT) has been used now for more than thirty years to determine mechanical properties from miniaturized samples. The use of small samples becomes necessary if a sufficient amount of material for the production of standard sized samples is not available.

The SPT is used in different sizes and different types. The smallest specimens are standard TEM sized specimen [1,2]. Other authors use specimens cut from remnants of CHARPY specimens, which are square shaped [3–5]. There has been a lot of effort to standardize the SPT and its usage [6], but this is still a running process. At least, there is a common understanding about the important features of the test.

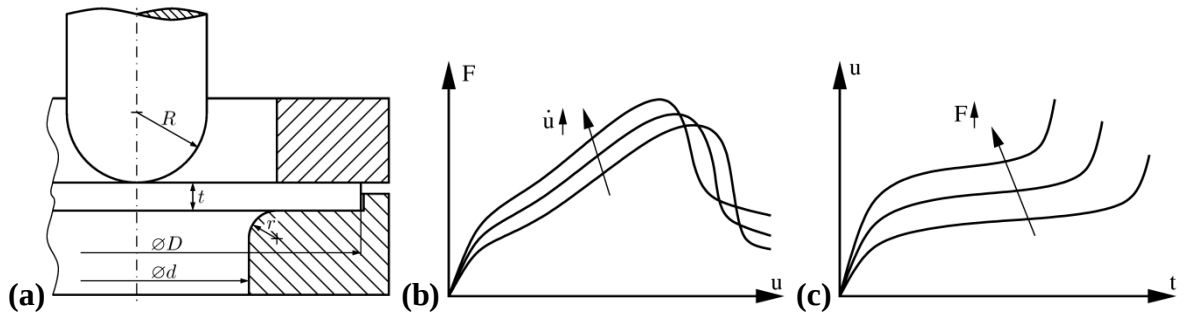

Figure 1. (a) Scheme of a SPT loading device and typical results for the different types of the SPT. (b) CDR-SPT and (c) CF-SPT for a visco-plastic metallic material with a strain induced damage evolution.

A disk or square shaped specimen with a diameter or length D and a thickness t is placed on a circular die with a receiving hole of diameter d. This receiving die can have a rounded or straight chamfer edge of size r. The specimen can be clamped between the receiving die and a down-holder. There are also cases where the specimen is not clamped, usually for testing very brittle materials to avoid initial deformations during clamping. The specimen is loaded centrically using a punch with a spherical tip of radius R. The loading can be a constant displacement rate (CDR) of the punch or a constant force (CF) applied to the punch followed by a holding (creep) time. The experimental results of the test are usually the punch displacement and/or the specimen deflection u and the punch force F. In case of time dependent material behaviour these values are stored together with the time t after starting the test. Figure 1(a) shows the typical test set-up and results for the different types of the SPT considering elastic, visco-plastic material with strain induced damage evolution.

The CDR-SPT can be performed at different punch velocities or specimen deflection rates. The result as shown in Figure 1(b) is a load deflection curve (LDC), which starts with a short linear section related to the elastic response of the specimen, followed by a typical knee whose height is related to the initial yield strength of the tested material. The next part of the curve corresponds to the ductile and strain rate related hardening. The decreasing slope just

ahead of the force maximum indicates a localization of deformation and the onset of material damage. The increasing damage leads finally to a decreasing load bearing capacity of the material due to the failure of the specimen. There is a remaining force at the end of the test, which is due to the frictional force between the penetrating punch and the specimen. If the punch speed is increased the curve is shifted to higher forces due to the strain rate sensitivity and the onset of damage happens at smaller deflections [7].

The CF-SPT is used to determine the material creep behaviour at different loads (stresses). As in uniaxial tensile creep tests we distinguish three parts of the curve, which are related to primary, secondary and tertiary creep, see Figure 1(c) middle. The primary part of the curve is also influenced by some initial plastic deformation at rather high strain rates. The tertiary part is of course also influenced by a localization of deformation and increasing creep damage. For increasing test forces a higher mean specimen deflection will be observed together with decreasing failure times [8]. In contrast to tensile creep tests there is an initial plastic deformation within the specimen, which might have an influence on the subsequent creep behaviour.

The SPT has been applied to a lot of different materials. Numerous evaluation approaches have been developed to correlate SPT-results to those obtained by conventional (standard) specimens. But one important fact just recently came into focus, which is the friction between the different parts of the setup. There is a contact between specimen and receiving die, between specimen and downholder and most important between specimen and punch. The punch itself is somehow guided (not shown in Figure 1) to deform the specimen at its exact centre.

Now, the question is how the contact properties influence the test results. Only a few studies have been found in literature, which explicitly focus on this problem [9–13]. The aim of this paper is to fill some of the gaps and to give suggestions about optimal test setups and evaluation strategies.

2. Models

First, the models for this numerical study are introduced. The material model is composed additively using an elastic, a plastic and a visco-plastic part and could be extended considering material damage [7]. The geometrical models are based on a "perfect" setup and are then changed using imperfections, which might appear in "real" test setups.

2.1 Material model

For the numerical experiments two different material behaviours are considered. For the CDR-SPT an elastic-plastic material model is chosen, which is further extended to an elastic visco-plastic model to simulate CF-SPT experiments. Both models are used in a finite-element framework, where small elastic deformations but finite plastic deformations are considered.

2.1.1 Elastic plastic model

Since an incremental plasticity approach is used, the strain rate $\dot{\varepsilon}_{ij}$ is split into an elastic $\dot{\varepsilon}_{ij}^{\mathrm{el}}$ and a plastic part $\dot{\varepsilon}_{ij}^{\mathrm{pl}}$.

$$\dot{\varepsilon}_{ij} = \dot{\varepsilon}_{ij}^{\mathrm{el}} + \dot{\varepsilon}_{ij}^{\mathrm{pl}} \tag{1}$$

The stresses are computed using HOOKE's law

$$\dot{\sigma}_{ij} = C_{ijkl}\dot{\varepsilon}_{kl}^{\mathrm{el}}\,. \tag{2}$$

For isotropic elastic material the elastic stiffness tensor is defined as

$$C_{ijkl} = \frac{E}{3(1-2\nu)}\delta_{ij}\delta_{kl} + \frac{E}{2(1+\nu)}(\delta_{ik}\delta_{jl} + \delta_{il}\delta_{jk} - \frac{2}{3}\delta_{ij}\delta_{kl})\,, \tag{3}$$

where E denotes the elastic modulus and ν Poisson's ratio. The plastic strain rate is

$$\dot{\varepsilon}_{ij}^{\mathrm{pl}} = \dot{\lambda}\frac{\partial f}{\partial \sigma_{ij}}\,, \tag{4}$$

The yield condition is

$$f = q - \sigma_{eq}(\varepsilon_{eq}^{pl}) = 0 \tag{5}$$

with q denoting the plastic potential (von Mises stress)

$$q = \sqrt{s_{ij} s_{ij}} \qquad \text{with} \qquad s_{ij} = \sigma_{ij} - \frac{1}{3}\delta_{ij}\sigma_{ij} . \tag{6}$$

To model strain hardening the Voce hardening law is used

$$\sigma_{eq}(\varepsilon_{eq}^{pl}) = \sigma_0 + \sigma_1 \varepsilon_{eq}^{pl} + \sigma_2 \left\lfloor 1 - \exp\left(-n\varepsilon_{eq}^{pl}\right) \right\rfloor \tag{7}$$

with the initial yield stress σ_0, linear hardening modulus σ_1, non-linear hardening modulus σ_2 and the non-linear hardening exponent n.

2.1.2 Elastic visco-plastic material

For CF-SPT simulations the elastic-plastic material law is extended by a creep strain rate $\dot{\varepsilon}_{ij}^{cr}$.

$$\dot{\varepsilon}_{ij} = \dot{\varepsilon}_{ij}^{el} + \dot{\varepsilon}_{ij}^{pl} + \dot{\varepsilon}_{ij}^{cr} \tag{8}$$

The creep strain rate is modelled using a simple Norton power law

$$\dot{\varepsilon}_{ij}^{cr} = A q^m N_{ij} \tag{9}$$

with the parameters A and m and the direction of creep strain

$$N_{ij} = \frac{\partial q}{\partial \sigma_{ij}} . \tag{10}$$

2.1.3 Contact modelling and properties

The normal behaviour is simulated using "hard" contact enforced by the ABAQUS penalty method. The tangential behaviour follows COULOMB's friction law

$$F_t = \mu F_n , \tag{11}$$

where F_n denotes the normal force and μ the friction coefficient.

2.1.4 Material properties

A fictitious material is assumed having the material parameters listed in table 1. The parameters are chosen such that they are near to those of a high-strength steel.

Table 1. Material parameters.

E [MPa]	ν [-]	σ_0 [MPa]	σ_1 [MPa]	σ_2 [MPa]	n [-]	A [$s^{-1}MPa^{-1}$]	m [-]
210000	0.3	500	250	250	15	$1 \cdot 10^{-32}$	12

2.2 SPT setup

Figure 2(a) shows a cross section view of the reference model of a typical SPT set-up. The specimen (1) D=8mm, t=0.5mm is supported concentrically by the receiving die (2) with a bore diameter of d=4mm and a straight chamfer edge r=0.5mm x 45°. The punch (3) has a spherical tip with radius R=1.25mm and a thicker cylindrical part d=6mm, which is rounded at the top, where it comes in contact with the push plate (6). The punch is guided by a lower (4) and upper (5) guiding socket, both having a slightly larger inner diameter than the outer diameter of the punch. The diameter difference is 0.1mm in both cases. Receiving die and the two guidance sockets are rigidly fixed

in space. The contact pairs specimen – die , specimen – punch are modelled using COULOMB's friction model with a friction coefficient μ_2. The other two contact pairs punch – lower guidance and punch – upper guidance become relevant only if the punch is tilted, which will happen in real world conditions. This tilting of the punch results in one ore two additional active contact pairs, which will reduce the force effectively acting on the specimen. The friction coefficient here is μ_1.

Therefore, two imperfect models are used to simulate "real world" conditions. In model B receiving die, specimen and punch tip are aligned exactly concentric, but the punch is tilted such that it just touches the upper guiding socket. Model C accounts for a situation, where the punch tip is shifted horizontally until one side of the punch touches the wall of the lower guiding socket. Additionally, lower die and specimen are non-concentric to the punch tip. Here, the deformation of the specimen causes an additional horizontal force, acting at the punch, causing increasing contact forces between punch and lower guidance socket. The amount of non-concentricity is denoted by Δx.

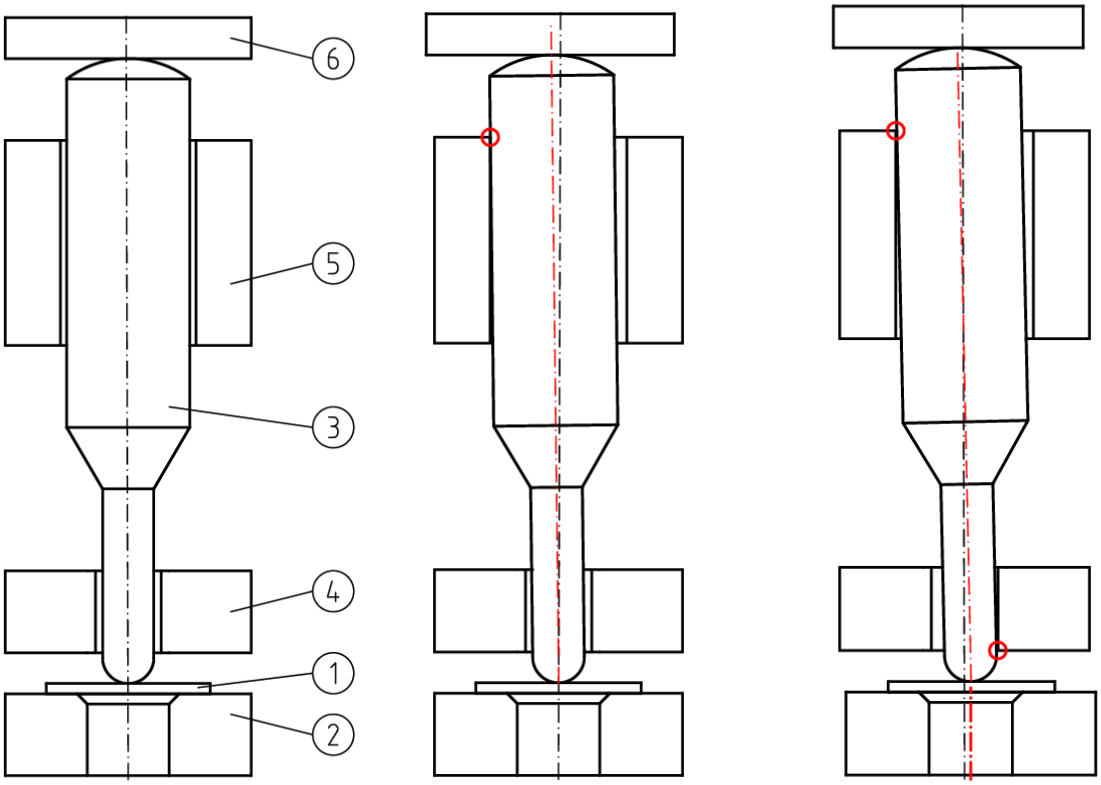

a) Model A **b)** Model B **c)** Model C

Figure 2. Model of the SPT, 1-specimen, 2-receiving die, 3-punch, 4-lower guidance, 5-upper guidance, 6-punching plate. **a)** Perfect Model; **b)** Friction between punch and upper guiding; **c)** Friction between punch and guiding and non-concentric receiving die. The red circles indicate contact locations.

3. Results

Tables 2 – 4 give an overview about the different cases that have been simulated. The first column denotes the number of the simulation, the second column corresponds to the model according to Figure 2, next three columns define the friction coefficients and shift Δx of the lower die and specimen, and the last column defines the test type (CDR: constant deflection rate, CF: constant force). For CDR-SPT simulations the maximum punch displacement is $u = 3.0$ mm and the load deflection curves are plotted. For CF-SPT simulations a punch force of $F = 350$ N is applied and the punch displacement is plotted over time.

3.1. Model A

Table 2. Simulated cases with model A.

Case	Model	μ_1	μ_2	Δx	Type
1	A	-	0.0	0.0	CDR
2	A	-	0.1	0.0	CDR
3	A	-	0.2	0.0	CDR
4	A	-	0.3	0.0	CDR
5	A	-	0.4	0.0	CDR
6	A	-	0.5	0.0	CDR
7	A	-	0.0	0.0	CF
8	A	-	0.1	0.0	CF
9	A	-	0.2	0.0	CF
10	A	-	0.3	0.0	CF
11	A	-	0.4	0.0	CF
12	A	-	0.5	0.0	CF

Model A considers only the contact between punch and specimen, which has the major influence on the results. Since this arrangement is axisymmetric, 2D-axisymmetric simulations are performed. Figure 3 shows on the left the load-deflection curves for the CDR-SPT. As long as the specimen deflection $u < 0.6$ mm, no friction effects are visible, because there is no sliding between punch and specimen. For specimen deflections $u > 0.6$ mm the influence of friction increases. The maximum load for a CDR-SPT with $\mu_2 = 0.5$ is about 30% higher with respect to test with $\mu_2 = 0.0$. For larger friction coefficients the maximum load occurs at larger specimen deflection. For CF-SPTs shown on the right side of Figure 3 the influence of the friction coefficient is even more severe with respect to the time of failure. No friction means a time of failure of 10000s whereas for a friction coefficient of 0.5 the time of failure reaches 370000s, which means an increase of 3700%.

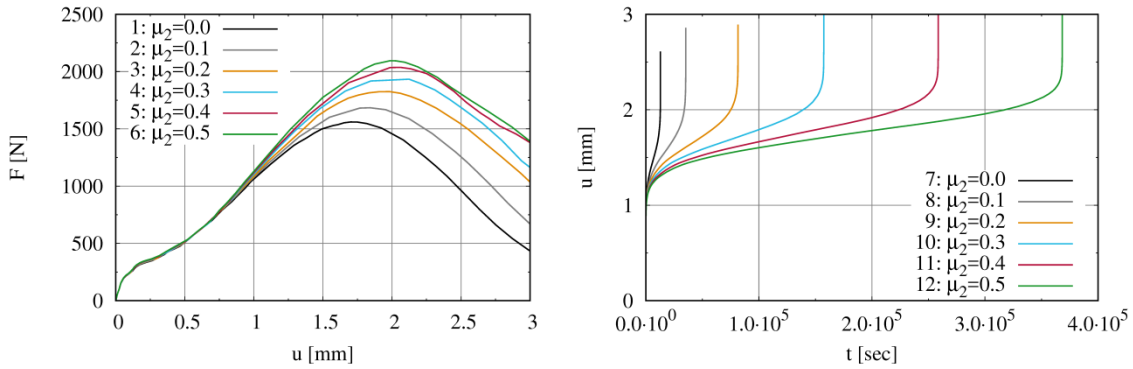

Figure 3. a) CDR-SPT, cases 1 – 6 ; **b)** CF-SPT, cases 7 – 12. Variation of friction coefficient μ_2 for the contact between punch and specimen. There is no contact between punch and guidance.

3.2 Model B

Table 3. Simulated cases with model B.

Case	Model	μ_1	μ_2	Δx	Type
13	B	0.0	0.2	0.0	CDR
14	B	0.1	0.2	0.0	CDR
15	B	0.2	0.2	0.0	CDR
16	B	0.3	0.2	0.0	CDR
17	B	0.4	0.2	0.0	CDR
18	B	0.5	0.2	0.0	CDR
19	B	0.0	0.2	0.0	CF
20	B	0.1	0.2	0.0	CF

21	B	0.2	0.2	0.0	CF
22	B	0.3	0.2	0.0	CF
23	B	0.4	0.2	0.0	CF
24	B	0.5	0.2	0.0	CF

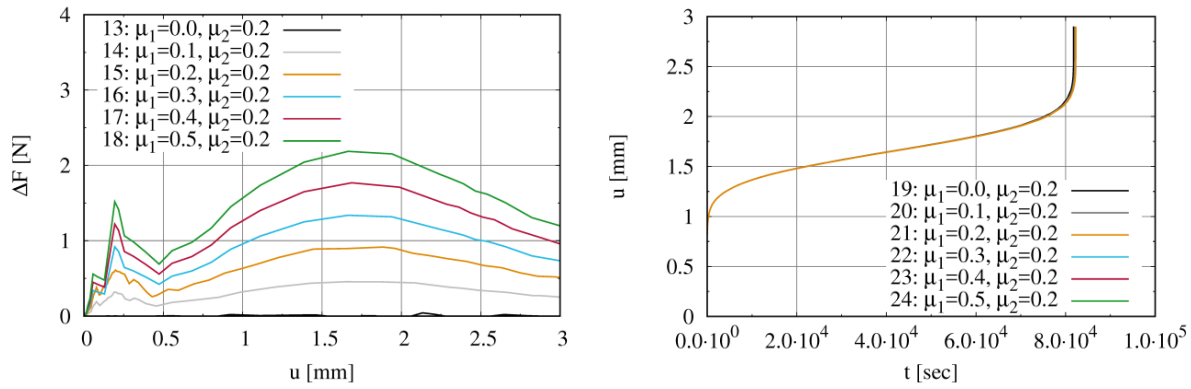

Figure 4. a) CDR-SPT, cases 13 – 18; **b)** CF-SPT, cases 19 – 24. Variation of the friction coefficient μ_1 for the contact between punch and guidance, friction coefficient $\mu_2 = 0.2 = \text{const.}$ for the contact between punch and specimen.

Model B considers in contrast to model A an additional contact between punch and the upper guiding assuming that the punch is slightly tilted, as depicted in Figure 2(b). These second contact generates an upward pointing frictional force, which effectively reduces the punch force acting on the specimen. This reduction ΔF is shown on the left hand side in Figure 4. It is around 1% of the current punch force. The CF-SPT results of these simulations are shown on the right in Figure 4. Such a small reductions of the punch force reduce the time of failure not significantly.

3.3 Model C

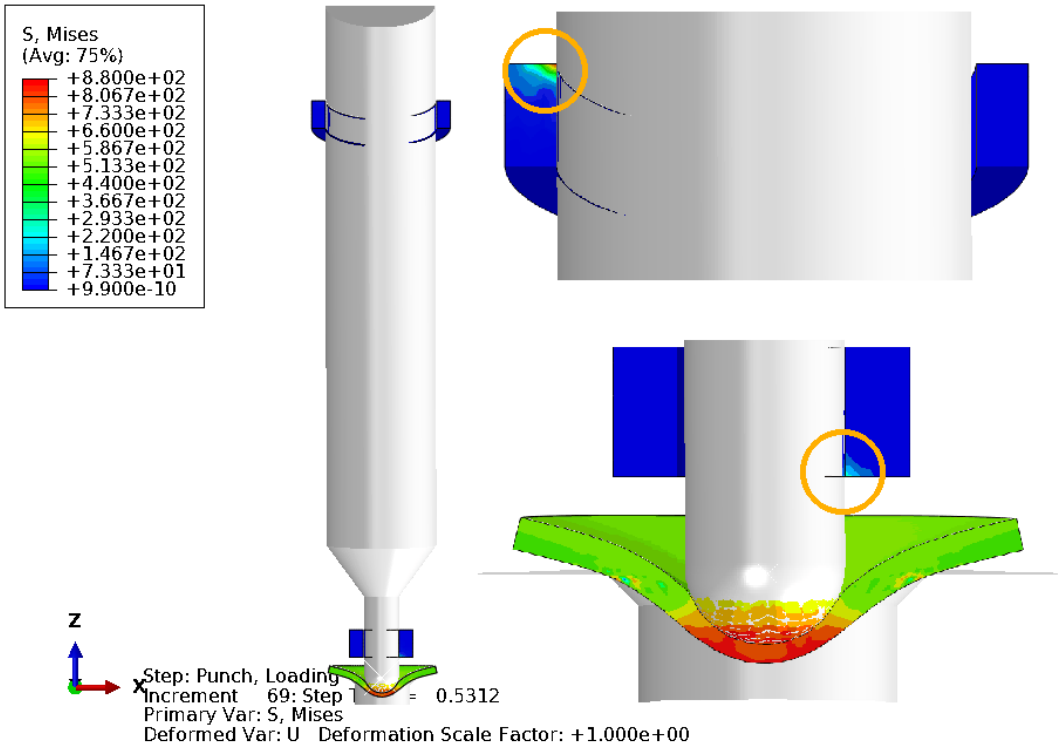

Figure 5. ABAQUS Model C. The orange circles show the two locations where the punch touches the guidance.

Table 4. Simulated cases using model C.

Case	Model	μ_1	μ_2	Δx	Type
25	C	0.1	0.2	0.0	CDR
26	C	0.1	0.2	0.1	CDR
27	C	0.1	0.2	0.2	CDR
28	C	0.2	0.2	0.0	CDR
29	C	0.2	0.2	0.1	CDR
30	C	0.2	0.2	0.2	CDR
31	C	0.3	0.2	0.0	CDR
32	C	0.3	0.2	0.1	CDR
33	C	0.3	0.2	0.2	CDR
34	C	0.4	0.2	0.0	CDR
35	C	0.4	0.2	0.1	CDR
36	C	0.4	0.2	0.2	CDR
37	C	0.5	0.2	0.0	CDR
38	C	0.5	0.2	0.1	CDR
39	C	0.5	0.2	0.2	CDR
40	C	0.0	0.2	0.1	CF
41	C	0.1	0.2	0.1	CF
42	C	0.2	0.2	0.1	CF
43	C	0.0	0.2	0.2	CF
44	C	0.1	0.2	0.2	CF
45	C	0.2	0.2	0.2	CF

In model C the punch is tilted such that it touches the upper guidance at the left and the lower guidance at the right side. Additionally the specimen and receiving die can be shifted to the right by Δx. Then, the specimen is loaded non-concentric, which results in an additional horizontal force acting on the punch and increasing the contact pressure and therewith the friction forces. Figure 5 shows the model in detail. The friction coefficient between specimen and punch is kept constant $\mu_2 = 0.2$, whereas the friction coefficient for the contact between punch and guidance μ_1 is varied. Figure 6 – 10 show on the left side the load-displacement curve of the punch and on the right side the force reduction due to the friction between punch and its guidance.

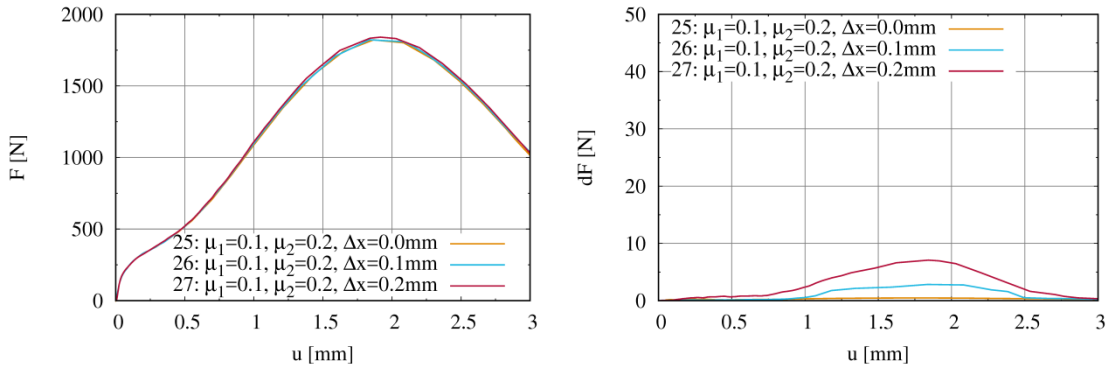

Figure 6. CDR-SPT cases 25 – 27. Variation of non-concentricity of die and specimen Δx, $\mu_1 = 0.1$, $\mu_2 = 0.2$.

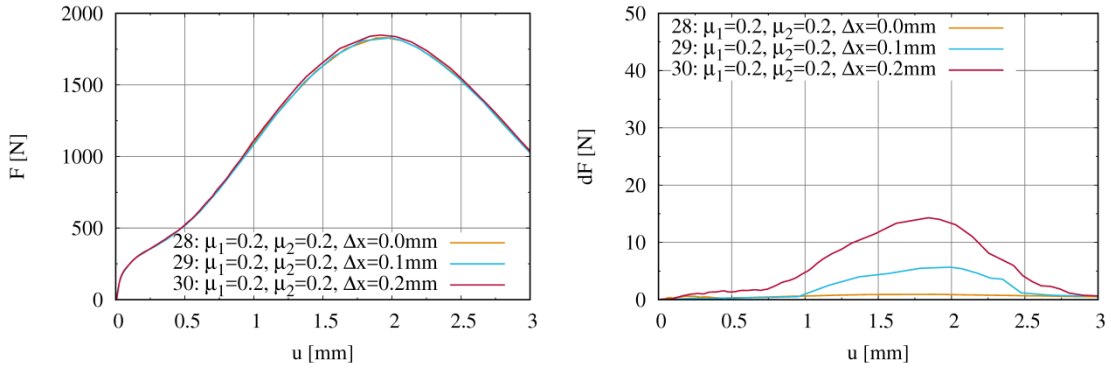

Figure 7. CDR-SPT cases 28 – 30. Variation of non-concentricity of die and specimen Δx, $\mu_1 = 0.2$, $\mu_2 = 0.2$.

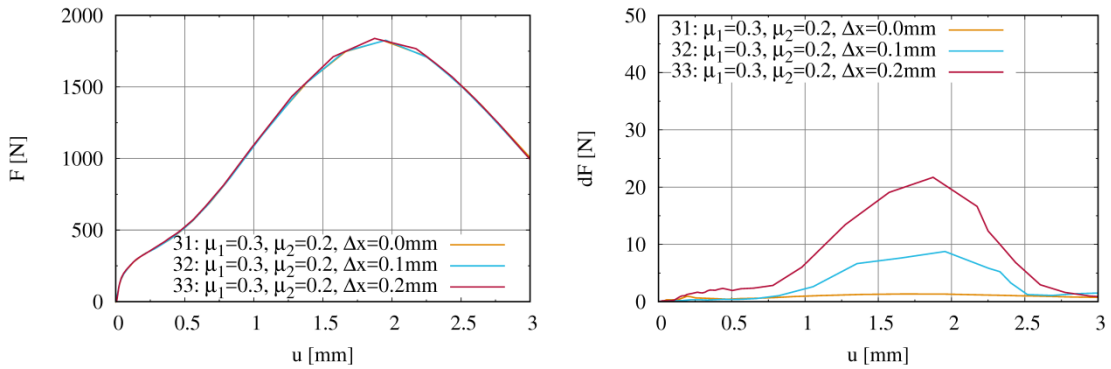

Figure 8. CDR-SPT cases 31 – 33. Variation of non-concentricity of die and specimen Δx, $\mu_1 = 0.3$, $\mu_2 = 0.2$.

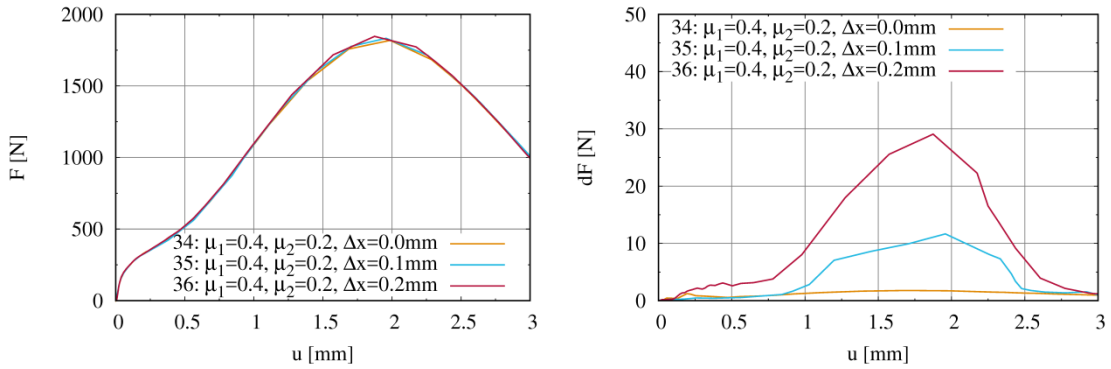

Figure 9. CDR-SPT cases 34 – 36. Variation of non-concentricity of die and specimen Δx, $\mu_1 = 0.4$, $\mu_2 = 0.2$.

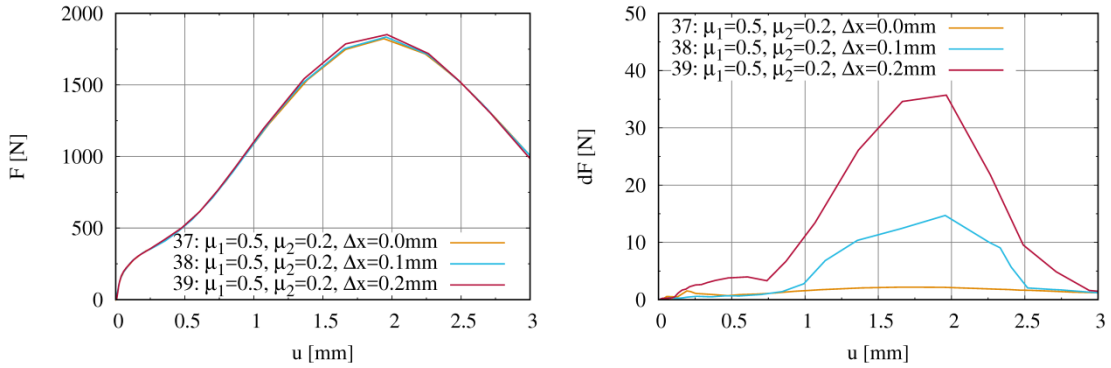

Figure 10. CDR-SPT cases 37 – 39. Variation of non-concentricity of die and specimen Δx, $\mu_1 = 0.5$, $\mu_2 = 0.2$.

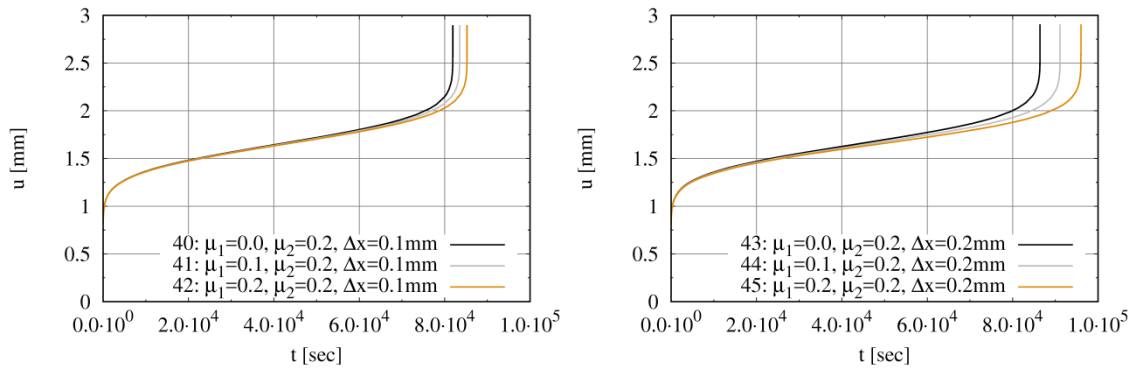

Figure 11. a) CF-SPT, cases 40 – 42, $\Delta x = 0.1$ mm**; b)** CF-SPT, cases 43 – 45, $\Delta x = 0.2$ mm. Variation of the friction coefficient μ_1 for the contact between punch and guidance, friction coefficient $\mu_2 = 0.2 = \text{const.}$ for the contact between punch and specimen.

For the CF-SPT the force reduction in model C has a visible effect and can increase the time of failure by 10%.

3.4 Specimen thickness reduction

As seen in section 3.1, the friction between specimen and punch has a significant effect in both test types CDR- and CF-SPT. Therefore, the friction coefficient becomes an important parameter within the model. To be able to identify material parameters using curve fitting algorithms the friction coefficient should be known, which raises the question how to identify this parameter. Figure 12 shows results from 2D-axisymmetric CDR-SPT simulations (model A) where the friction coefficient is varied between 0.0 and 0.5. For increasing friction coefficients the remaining central specimen thickness also increases. Figure 13 shows the reduction of the central specimen thickness Δt for both CDR- and CF-SPT as function of the punch displacement. Until $u = 2$ mm only small deviations between the two test types are observed. If the thickness reduction can be measured exactly the important friction coefficient μ_2 can be estimated, as shown at the right hand side in Figure 14, where experiment and simulation are compared for a single 9Cr specimen with an identified friction coefficient $\mu_2 = 0.26$. u_{top} denotes the punch deflection and u_{bot} the central specimen deflection. The left diagram in Figure 14 shows experiments on 9Cr specimen in comparison with simulations with varying friction coefficient. These results suggest that the friction coefficient may vary between 0.2 and 0.4 for this particular test setup. The punch material in this setup is a polished fully hardened stainless steel.

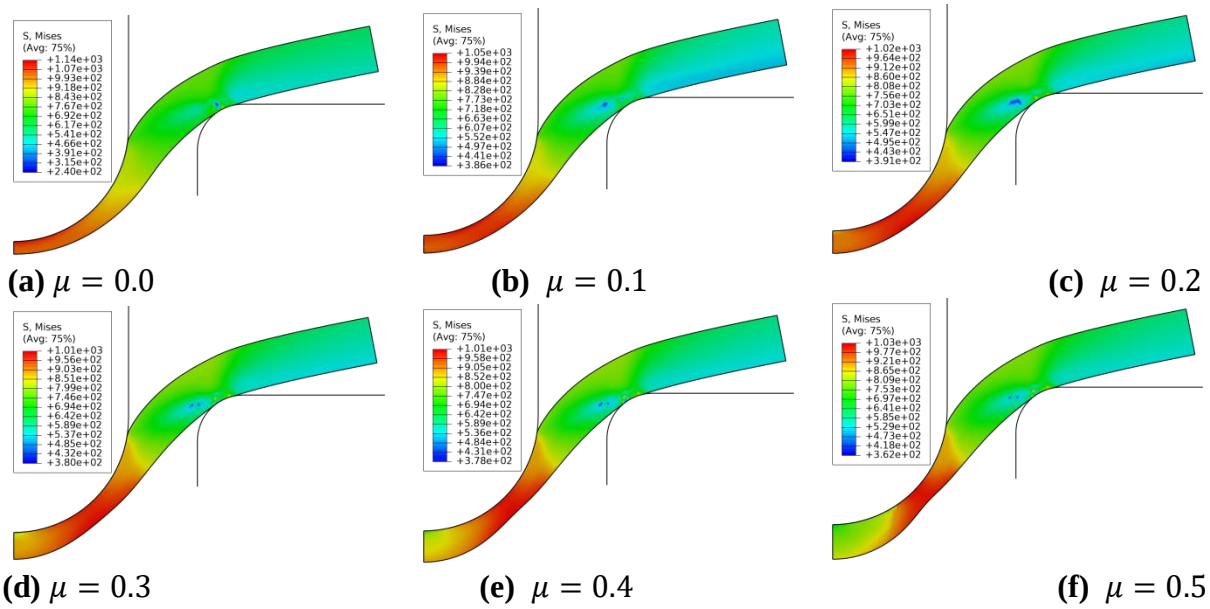

Figure 12. CDR-SPT, cases 1 – 6. Reduction of the central specimen thickness for model A for a constant deflection $u = 2$ mm. Variation of the friction coefficient $\mu_2 = 0.0 \ldots 0.5$ for the contact between punch and specimen.

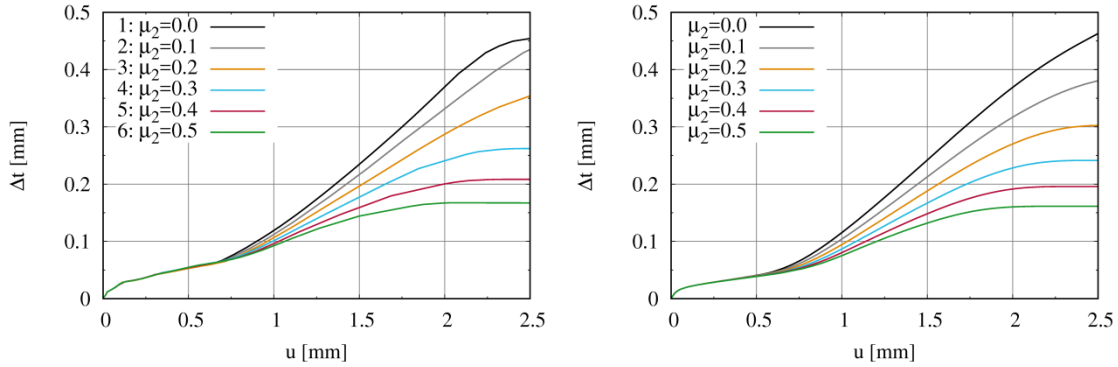

Figure 13. a) CDR-SPT; **b)** CF-SPT. Reduction of central specimen thickness for model A. Variation of the friction coefficient μ_2 for the contact between punch and specimen.

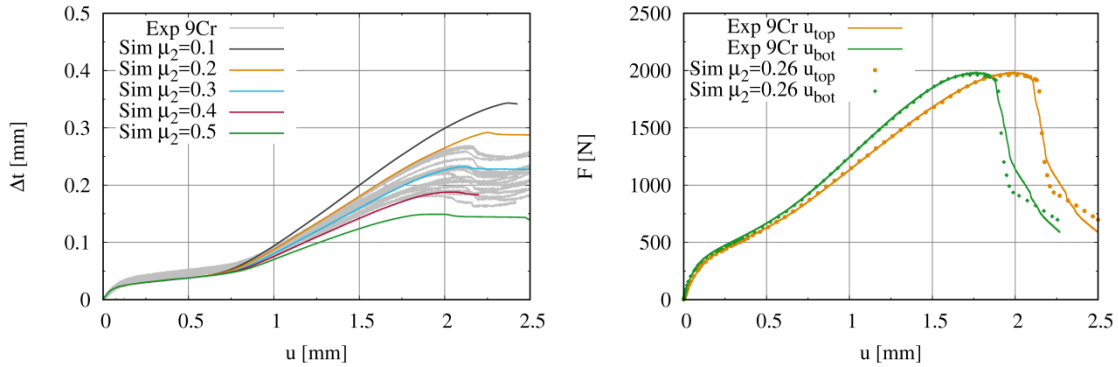

Figure 14. a) Comparison between experiments and simulations on 9Cr-Steel. **b)** Comparison of experiment and simulation for a single specimen with identified friction coefficient.

4. Conclusions

This numerical study shows the importance of friction effects in CDR- and CF-SPTs. The friction between punch and its guidance could be controlled by an exact alignment of the setup and a proper lubrication of the punch. Then these effects might be neglectable. But the friction between specimen and punch can't be avoided and must be therefore taken into account during test evaluation. One method to determine the friction coefficient is the continuous measurement of the central specimen thickness during testing. The thickness reduction is mainly controlled by friction, but not totally independent from the material behaviour, why a precise simulation using a proper material law is necessary to identify friction coefficients. Especially in CF-SPTs at elevated temperatures, the friction coefficient might depend on temperature, punch force, testing time and punch and specimen material, which makes the identification of the friction coefficient a challenging task.

Acknowledgments: The authors gratefully acknowledge the financial support by the German Research Foundation (DFG) within the collaborative research centre SFB 920.

References

1. Manahan, M.P.; Argon, A.S.; Harling, O.K. The development of a miniaturized disk bend test for the determination of postirradiation mechanical properties. *Journal of Nuclear Materials*, 103:1545-1550, 1981.
2. Kameda, J. and Mao, X. Small-punch and TEM-disc testing techniques and their application to characterization of radiation damage. *Journal of Materials Science*, 27(4):983-989, 1992.
3. Baik, J.M.; Kameda, J; Buck, O. Small Punch Test evaluation of intergranular embrittlement of an alloy steel. *Script Metallurgica*, 17:1443-1447, 1983.
4. Baik, J.M.; Kameda, J.; Buck. O. Development of small punch tests for ductile-brittle transition temperature measurement of temper embrittled Ni-Cr steels. In *The use of small-scale specimens for testing irradiated material*, W.R. Corwin, G.E. Lucas, editors, pp. 92-111. ASTM STP 888, Philadelphia, PA, 1986.
5. Linse, T.; Kuna, M..; Schuhknecht, J.; Viehrig. H.-W. Application of the Small-Punch Test to Irradiated Reactor Vessel Steels in the Brittle-Ductile Transition Region. *Journal of ASTM International*, 5(4):1-14, 2008.
6. CEN. Workshop Agreement CWA 15627:2006, *Small Punch Test method for Metallic Materials*. Technical report, Brussels, Belgium, 2006.
7. Abendroth, M.; Kuna. M. Identification of ductile damage and fracture parameters from the small punch test using neural networks. *Engineering Fracture Mechanics*, 73(6):710-725, 2006.
8. Dymacek, P.; Milicka. K. Creep small-punch testing and its numerical simulations. *Materials Science and Engineering A*, 510-511:444-449, 2009.
9. Andres, D.; Dymacek. P. Study of the upper die clamping conditions in the small punch test. *Theoretical and Applied Fracture Mechanics*, 86:117-123, 2016.
10. Cacciapuoti, B.; Sun, W.; McCartney. D.G. A study on the evolution of the contact angle of small punch creep test of ductile materials. *International Journal of Pressure Vessels and Piping*, 145:60-74, 2016.
11. Fa-Kun, Z.; Guo-Yan, Z.; Shan-Tung. T. Numerical investigation of frictional effect on measuring accuracy of different small specimen creep tests. *International Journal of Pressure Vessels and Piping*, 110:42{49, 2013.
12. Zhang, L.; Min, J.; Carsley, J.; Stoughton, T.B.; Lin. J. Experimental and theoretical investigation on the role of friction in Nakazima testing. *International Journal of Mechanical Sciences*, 133:217-226, 2017.
13. Selent, M.; Abendroth, M.; Kuna. M. Experimental and Numerical Investigations on the Creep Behaviour of Heat-Resisting Chromium Steel X10CrMoVNb9-1 by Means of Small Punch Test. *Transactions of the Indian Institute of Metals*, 69:629-633, 2016.